Science Advances
AAAS

advances.sciencemag.org/cgi/content/full/3/2/e1602498/DC1

Supplementary Materials for

Long-range allosteric signaling in red light–regulated diguanylyl cyclases

Geoffrey Gourinchas, Stefan Etzl, Christoph Göbl, Uršula Vide, Tobias Madl, Andreas Winkler

Published 3 March 2017, *Sci. Adv.* **3**, e1602498 (2017)
DOI: 10.1126/sciadv.1602498

The PDF file includes:

Other Supplementary Material for this manuscript includes the following:
(available at advances.sciencemag.org/cgi/content/full/3/2/e1602498/DC1)

- movie S1 (.mp4 format). Changes in conformational dynamics upon red light illumination of *Is*PadC.

- movie S2 (.mp4 format). Changes in conformational dynamics upon red light illumination of the *Is*PadC PSMcc variant.
- movie S3 (.mp4 format). The influence of effector deletion on conformational dynamics of the dark-state *Is*PadC PSMcc assembly.
- movie S4 (.mp4 format). The influence of effector deletion on conformational dynamics of the light-state *Is*PadC PSMcc assembly.

Supplementary Results

Detailed comparison of different IsPadC crystal structures

Previously crystallized photosensory modules (PSM) of various phytochromes feature a high diversity of dimeric PAS-GAF-PHY arrangements. Therefore, we addressed the relative energetic contribution of individual domains to the full-length parallel *Is*PadC dimer interface by performing a PISA analysis (*62*). Interestingly, the calculated ΔG^{diss} values, which indicate the free energy of assembly dissociation, revealed that a major contribution to the overall stability of the assembly is provided by the coiled-coil linker (residues 501-528, ΔG^{diss} = 8.0 kcal mol^{-1}). The sum of additional contacts provided by the PSM altogether (residues 8-500, ΔG^{diss} = 8.8 kcal mol^{-1}) contribute only to a similar extent to the overall stability of the phytochrome dimer (PAS-GAF-PHY-coiled-coil, ΔG^{diss} = 22.6 kcal mol^{-1}). Therefore, the absence of helical elements continuing from the C-terminal PHY helix in most of the previously crystallized PSM modules is one reason for the observation of antiparallel assemblies as well as the structural plasticity of parallel phytochrome dimers (Fig. 4).

The dimeric *Is*PadC assembly shows a two-fold symmetry for the PSM module and the superposition of the non-crystallographic symmetry related monomers of the full-length molecule (RMSD of 0.65 Å over 452 Cα-atoms for the PSM alignment) reveals that the individual protomers are almost identical. However, the global symmetry is disturbed by a bending of the coiled-coil linker and an asymmetric dimer interface of the GGDEF domains. Considering the lack of significant interactions between the two GGDEF protomers (ΔG^{diss} = -11.8 kcal mol^{-1} for residues 529-683) their relative positioning appears to be mainly influenced by contacts with neighboring GGDEF molecules in the crystal lattice. The global asymmetry is also translated to the local residue level for Arg538, Arg539, His577 and Asp659 at the GGDEF interface, which are all residues close to the expected GTP binding site. Interestingly, this local structural asymmetry can also be observed for several residues along the central helical spine, for instance Phe132 at the GAF dimer interface, Met320 within the internal helical connector of the GAF and PHY domains and Arg493 at the PHY dimer interface. Since our HDX-MS data support a functional coupling between DGC activity and the coiled-coil linker as well as the central helical spine (Fig. 2), the observed asymmetry of individual residues at the dimer interface could indicate their involvement in signal integration and communication. However, these residues are not highly conserved (fig. S1) and, therefore, their asymmetry might rather reflect an overall property of the central helical spine than any specific interactions. Interestingly, comparing these residues to their counterparts in the PSMcc structure lacking the overall asymmetry of linker and the GGDEF domains reveals that the local asymmetry is absent for Met320 and Arg493 in both PSM dimers.

Apart from the lack of local asymmetry in the central helical spine, the PSMcc monomers are almost identical to the PSM fragments of the full-length structure (except for the different architecture of the tongue element in chain D of the PSMcc structure – see main text). By superimposing the different protomers with the PAS-GAF core domain of the full-length molecule (RMSD = 0.28 Å, 0.27 Å, 0.30 Å and 0.57 over at least 234 Cα-atoms for monomers A, B, C and D, respectively), we observe a similar subtle displacement of the PHY domains in the aligned protomers as well as some flexibility of the dimer interface as seen for different phytochrome assemblies (Fig. 4). However, the amplitude of the structural rearrangements is less pronounced, as would be expected due to the presence of part of the coiled-coil linker extending from the core PHY domain. Performing the same analysis with the GTP soaked structure reveals that the PSM modules are almost unaffected by GTP binding in the GGDEF domain, most likely, because of crystal lattice restraints (RMSD = 0.38 Å over 433 α-carbon for the PSM superposition). Nevertheless, the observed more pronounced bending of the coiled-coil linker also results in subtle structural rearrangements of the PHY domains relative to the full-length structure in the absence of GTP. This bending is induced by a rearrangement of the GGDEF dimer interface that upon GTP binding attains an almost perfect 2-fold symmetry. Establishing this symmetric assembly requires a repositioning of the GGDEF dimer within the overall crystal lattice and, while the PSM module is held tightly in place, the linker apparently has enough flexibility to adapt to the new environment. Since the PSM module is apparently fixed by the crystal restraints, also the local asymmetry of residues Phe132, Met320 and Arg493 is still present even though the GGDEF asymmetry is absent. The symmetric arrangement of the GGDEF dimer is driven by a closing of the binding sites around the GTP molecules. For instance Asp581 and Arg603 interact with the guanosine base and Arg537 from the symmetry related monomer contacts GTP via a cation-pi interaction. Interestingly, additional important residues contributing to the GGDEF dimer interface (Asp663, His577 and Tyr670) show structural differences when comparing the full-length structure with the GTP soak. The Tyr670 rearrangement is particularly interesting because it enables access of GTP to its binding site. Having a closer look at the highly conserved GG(D/E)EF sequence in the half-active site in GTPαS bound GGDEF structures (*21*, *63*) shows a sampling of various configurations for the (D/E) and the E residues. The (D/E) residues are always involved in the Mg^{2+} coordination with the substrate, however, in the GTP soaked *Is*PadC structure it adopts a different conformation compared to the GTPαS bound structures to interact with the GTP α-phosphate that also contacts the Mg^{2+} ion. The conserved (D/E) residue is in proximity to the hydroxyl group of the ribose group of the non-crystallography symmetry related substrate molecule, and might therefore be involved in the interaction with the substrate and controlling the further closing of the active site required for product formation.

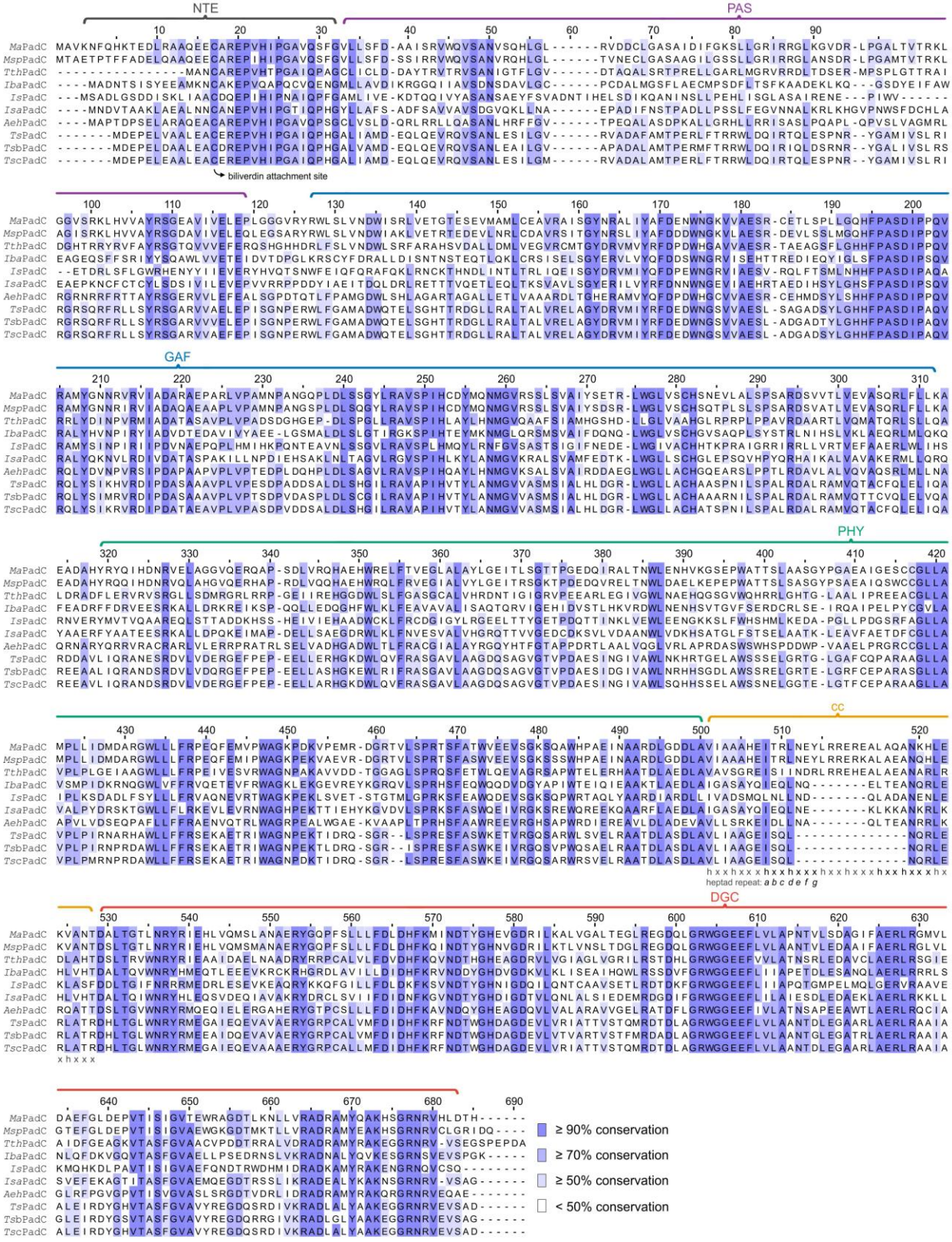
NTE
PAS
biliverdin attachment site
GAF
PHY
cc
DGC
MaPadC
MspPadC
TthPadC
IbaPadC
IsPadC
IsaPadC
AehPadC
TsPadC
TsbPadC
TscPadC
heptad repeat: a b c d e f g
≥ 90% conservation
≥ 70% conservation
≥ 50% conservation
< 50% conservation

fig. S1. Multiple sequence alignment of PadC homologs generated with Jalview (*64*). Numbering corresponds to the PadC homolog from *Idiomarina* species A28L (*Is*PadC) and indicated domain boundaries are based on structural features of the corresponding full-length structure with individual domains colored according to Fig. 1. The conserved biliverdin attachment site and the heptad repeat units of the coiled-coil linker region are indicated. Individual residues are highlighted in shades of blue according to their degree of conservation as indicated in the legend. Abbreviations of individual organisms and RefSeq accession numbers of the corresponding proteins read as follows: *Ma – Marinimicrobium agarilyticum* and WP_027329460 ; *Msp – Marinimicrobium* species LS-A18 and WP_036160751; *Tth – Thioalkalivibrio thiocyanodenitrificans* and WP_051079936; *Iba – Idiomarina baltica* and WP_006955969; *Is – Idiomarina* species A28L and WP_007419415; *Isa – Idiomarina salinarum* and WP_034774458; *Aeh – Alkalilimnicola ehrlichii* and WP_011629241; *Ts – Thioalkalivibrio* species ALMg3 and WP_026331574; *Tsb – Thioalkalivibrio* species AKL8 and WP_026304848; *Tsc – Thioalkalivibrio species* ALMg11 and WP_018949990, respectively.

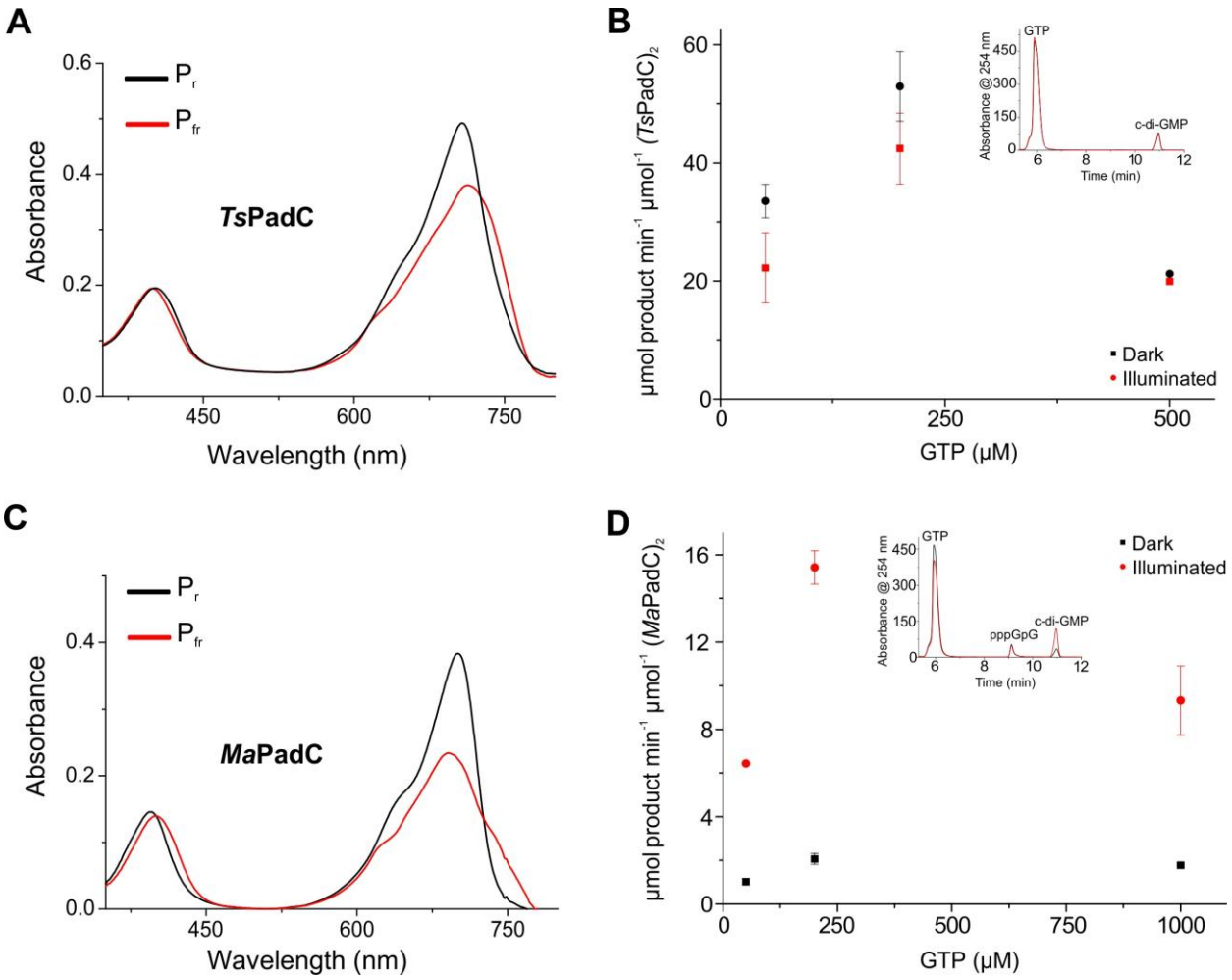

fig. S2. Spectroscopic and kinetic characterization of *Ts*PadC and *Ma*PadC. (**A** and **B**) UV-Vis spectra of dark-adapted samples and after red light irradiation of *Ts*PadC (A) and *Ma*PadC (B). (**C** and **D**) Kinetic characterization of product formation for *Ts*PadC (C) and *Ma*PadC (D). Product formation was quantified in triplicate for several reaction times and the standard deviation of individual points contributed to the error estimation of the linear fit that is used to calculate the initial rate of product formation. The standard error of the estimate from the linear regression is shown as error bar for each GTP concentration. Light-state data of all experiments are shown in red while dark-state data are represented in black.

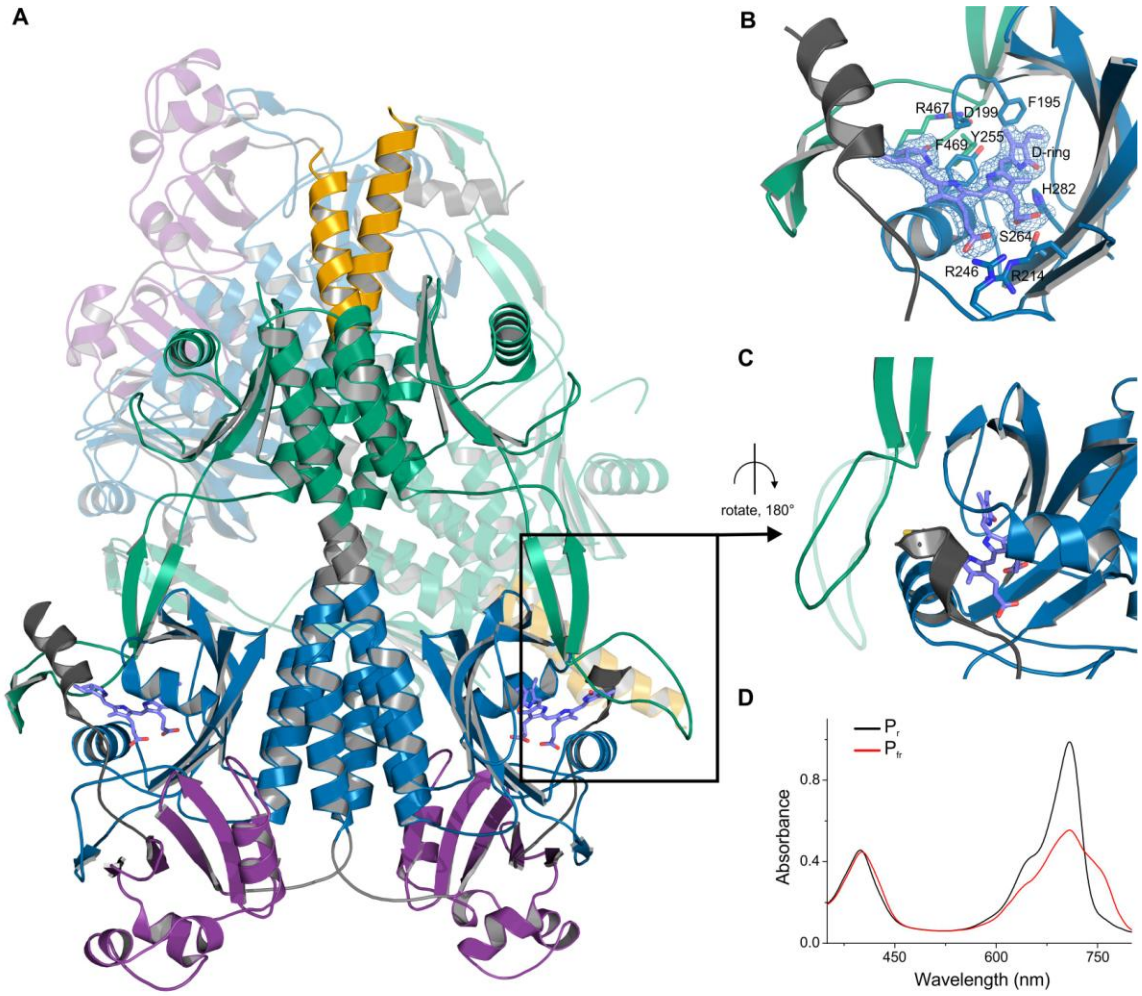

fig. S3. Characterization of the *Is*PadC PSMcc variant. (**A**) Cartoon representation of the asymmetric unit content of the crystallized PSMcc variant. The dimer of chains C and D is shown in forefront with individual domains colored in dark grey, violet, blue, green, and orange for the NTE, PAS, GAF, PHY, and coiled-coil domains, respectively. The biliverdin cofactor is shown as light blue stick model. Chains A and B in the background are shown in transparency. (**B**) Close up view of the biliverdin binding pocket of the higher resolution PSMcc structure with the same view as Fig. 2B. The $2F_o–F_c$ electron density map contoured at 1σ around the cofactor is shown as light blue mesh. Functionally relevant residues are shown as stick models. (**C**) Close up view of the PHY tongue region of monomer D. The view is rotated relative to panel A to better visualize the loss of the β–hairpin extension in the tongue region of chain D. Superposition with the conformation of the tongue region observed in all other chains (chain B shown in transparent mode for comparison) highlights the characteristic differences. These structural rearrangements are induced by crystal contacts with a neighboring molecule and support the conformational flexibility of the tongue region observed by HDX-MS (Fig. 2D). (**D**) UV-Vis spectra of *Is*PadC PSMcc in its dark-adapted state and after red light illumination reveal a similar P_{fr} to P_r ratio as for full-length *Is*PadC.

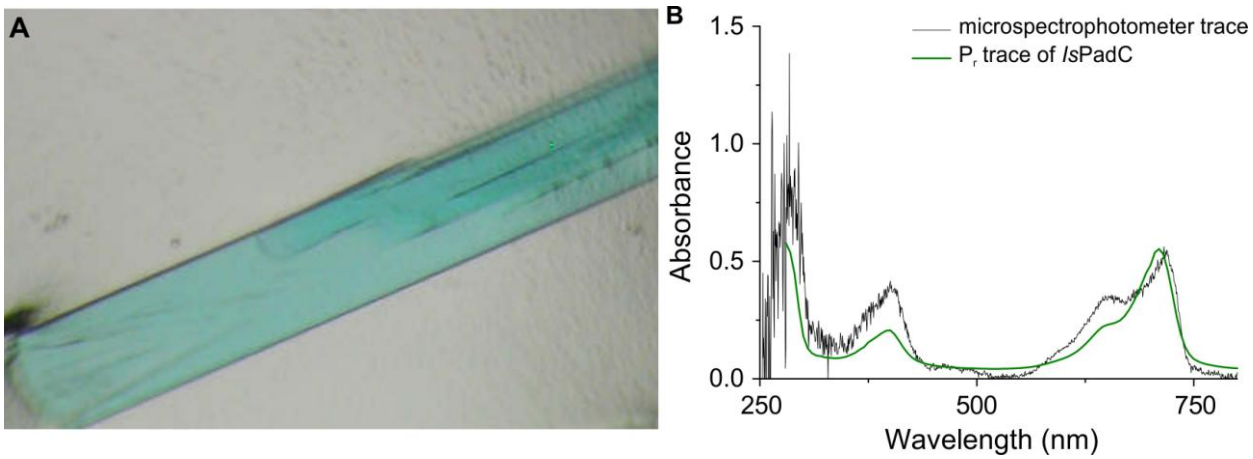

fig. S4. *Is*PadC crystal and spectral characteristics of dark-state crystallized *Is*PadC. (**A**) Representative crystal obtained during the crystallization of full-length *Is*PadC under dark conditions. (**B**) Comparison of a UV/Vis spectrum of crystalline *Is*PadC recorded with the microspectrophotometer at beamline ID30A-3 *(59)* with that obtained in solution. The comparison confirms that *Is*PadC has been crystallized in its dark-adapted P_r-state conformation.

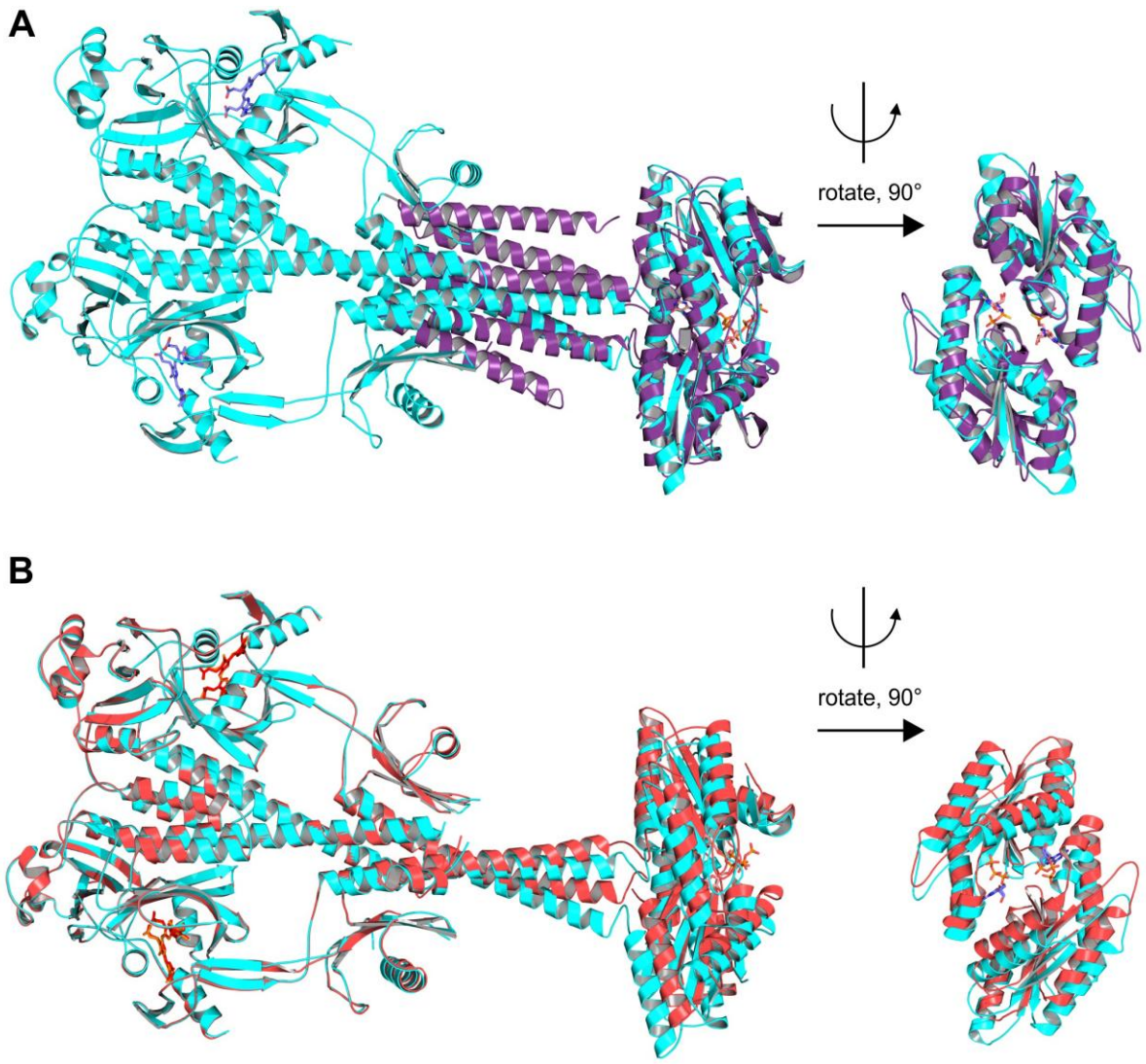

fig. S5. Effect of substrate binding on the overall architecture of *Is*PadC. (**A**) Structural alignment of the zinc-regulated diguanylyl cyclase DgcZ (colored in purple) with the DGC domain of full-length *Is*PadC (colored in cyan). The guanosine-5'-RP-α-thio-triphosphate (GAV) bound to DgcZ is shown as stick model. Individual DGC domains superpose very well (Root-mean-square deviation (rmsd) = 0.8 Å for 114 Cα atoms) and also the dimeric GGDEF arrangement is similar with an overall rmsd of 1.4 Å for 247 aligned Cα atoms. (**B**) Superposition of the full-length *Is*PadC structure obtained after GTP soaking (colored in red) with native *Is*PadC (colored in cyan). The two substrate molecules bound at the interface of the DGC dimer are shown as stick models. The superposition reveals a virtually identical PSM dimer (rmsd = 0.4 Å for 840 aligned Cα atoms) and only the linker region and the DGC dimerization show characteristic rearrangements upon GTP binding (rmsd = 2.0 Å for 306 Cα atoms of the dimeric DGC assembly) that are essentially restricted to a more pronounced bending of the coiled-coil linker coupled to a dimer rearrangement of the GGDEF domains that does not affect individual DGC domains (rmsd of 0.4 Å for 140 aligned Cα atoms in chain B).


A
Drel IsPadC(light) – Drel IsPadC(dark)
B
Drel IsPadC PSMcc(light) – Drel IsPadC PSMcc(dark)
C
Drel IsPadC(dark) – Drel IsPadC PSMcc(dark)
D
Drel IsPadC(light) – Drel IsPadC PSMcc(light)
≥1.5
≥0.9
≥0.3
<-0.3
<-0.9
<-1.5
ΔDrel
0
40
80
120
160
200
240
280
320
360
400
440
480
520
560
600
640
680

fig. S6. Summary of HDX experiments. A complete illustration of all *Is*PadC peptides evaluated by HDX is presented in panels A-D. Zoom in on the electronic version to reveal full details. Each box represents one peptide and contains up to five different colors that, from the bottom up, correspond to deuteration times of 10, 45, 180, 900 and 3,600 s, respectively. Individual colors correspond to the change in relative deuteration (ΔD_{rel}) of the two compared states according to the legend in the top left corner. MS^2 confirmed peptides are marked with diamonds. Terminal arrows at the end of a box indicate continuation of the peptide in the previous or following line. Secondary structure elements are taken from DSSP analysis of the corresponding structures and are colored according to the domain representation of Fig. 1A. A compilation of all individual deuteration plots for *Is*PadC and *Is*PadC PSMcc can be found in fig. S7. (**A**) Changes in *Is*PadC deuteration upon red-light illumination (also see movie S1). (**B**) Changes in *Is*PadC PSMcc deuteration upon red-light illumination (also see movie S2). (**C**) Changes in deuteration of *Is*PadC PSMcc compared to full length *Is*PadC in their dark-adapted states (also see movie S3). (**D**) Changes in deuterium uptake of the light-adapted states of *Is*PadC PSMcc compared to full length *Is*PadC (also see movie S4).

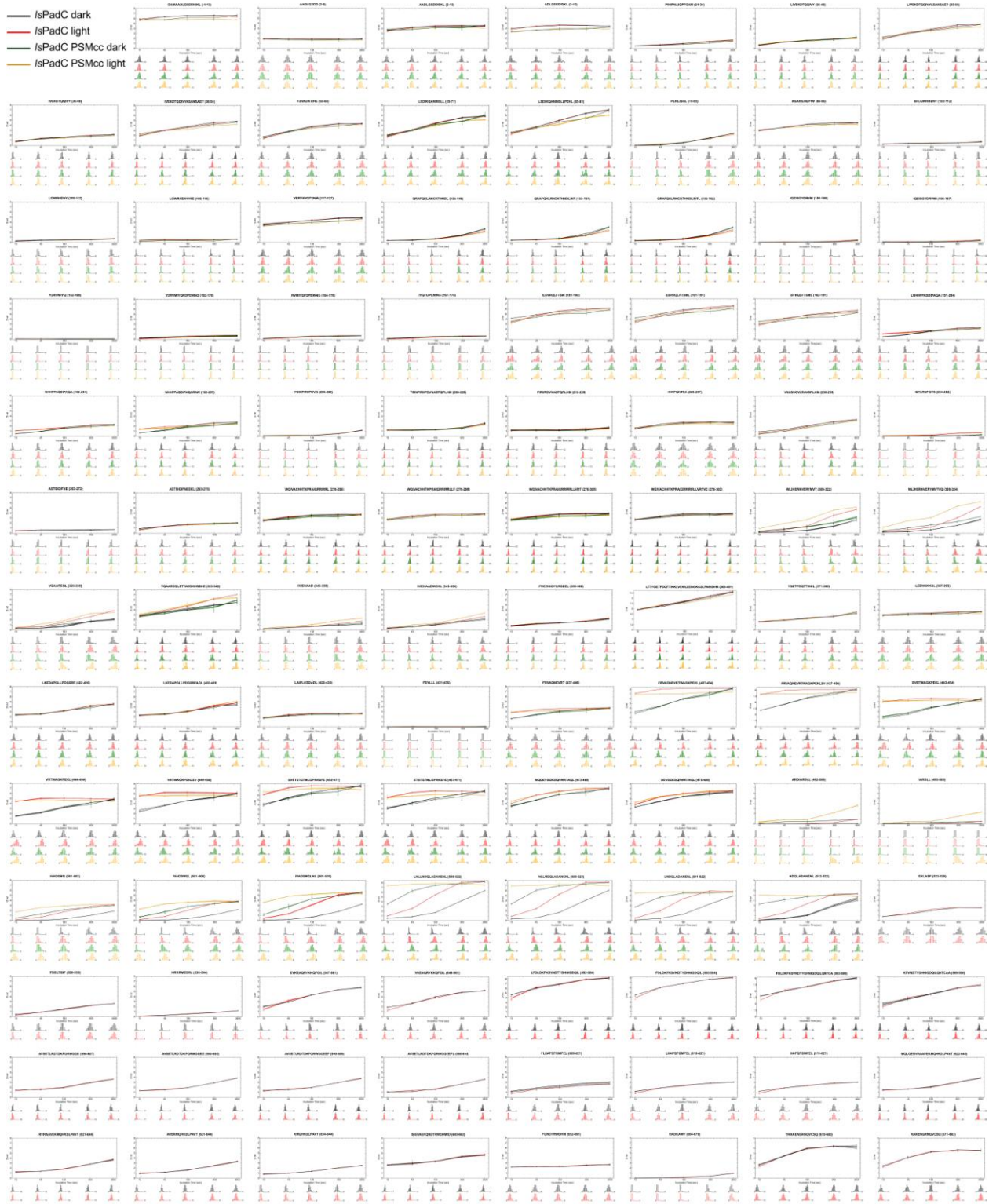
lsPadC dark
lsPadC light
lsPadC PSMcc dark
lsPadC PSMcc light

fig. S7. Individual deuterium incorporation plots of all evaluated peptides. Peptide sequences and their corresponding position according to the *Is*PadC sequence are shown on top of each sub-panel. Ordinates of each plot correspond to the relative deuterium incorporation and abscissae to the labeling time in seconds. *Is*PadC traces are colored in black and red corresponding to *Is*PadC in the dark- and light-state, Similarly, *Is*PadC PSMcc traces are colored in green and orange for the dark- and light-state, respectively. D_{rel} values are shown as the mean of three independent measurements and error bars correspond to the standard deviation. A software-estimated abundance distribution of deuterated species is presented in the lower sub-panel on a scale from undeuterated to all exchangeable amides deuterated. Zoom in on the figure in the electronic version for full details.

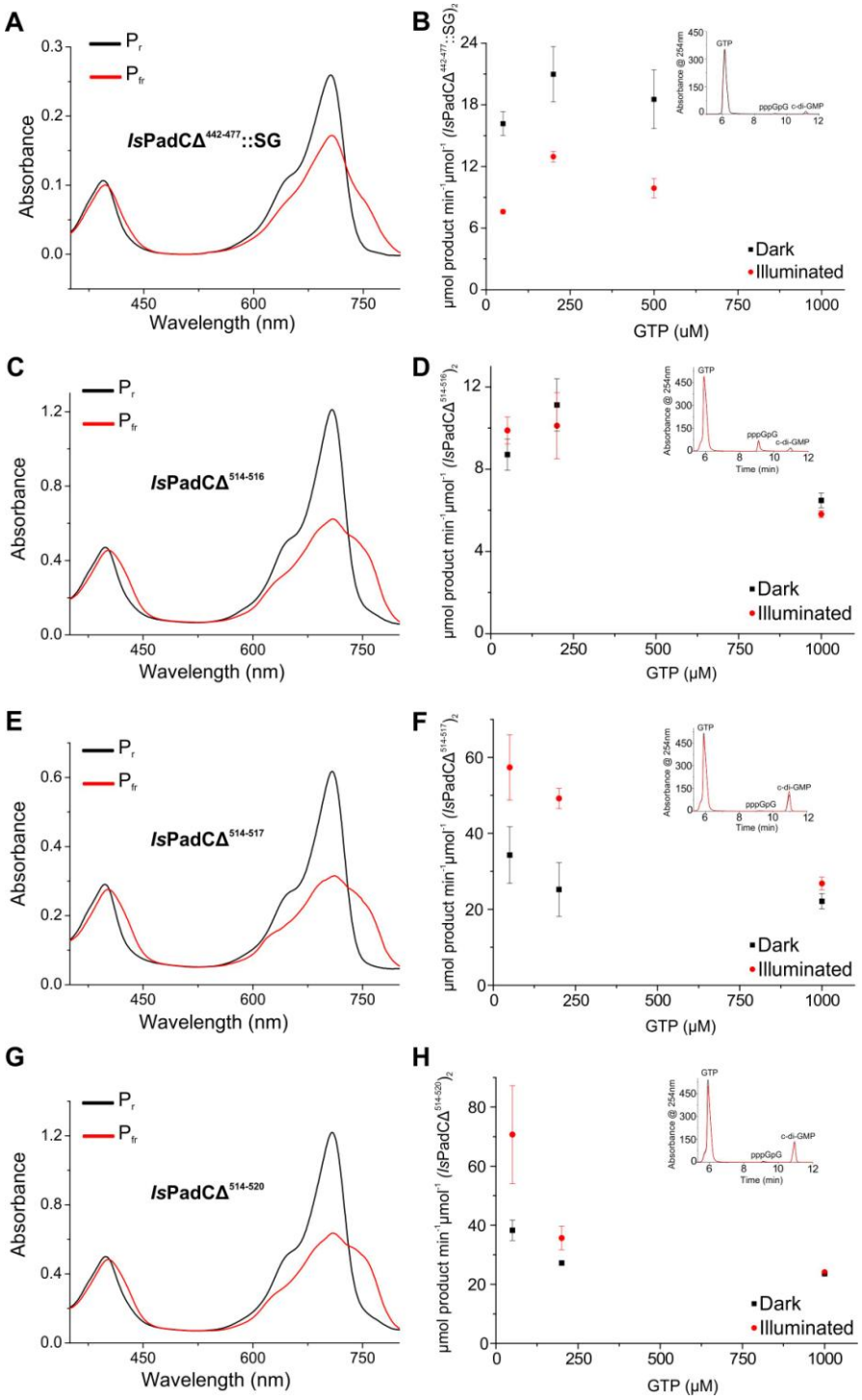

fig. S8. Spectroscopic and kinetic characterization of *Is*PadC deletion variants. UV-Vis spectra of different variants in their dark-adapted states (P_r, black lines) and after red light illumination (P_{fr}, red lines). The constructs shown correspond to deletions of the tongue region as well as deletion of 3, 4 and 7 residues in the coiled-coil region; *Is*PadC $\Delta^{442–477}$::SG (**A**), *Is*PadC $\Delta^{514–516}$ (**C**), *Is*PadC $\Delta^{514–517}$ (**E**) and *Is*PadC $\Delta^{514–520}$ (**G**), respectively. Panels B, D, F and H

show the results of the kinetic characterization of *Is*PadC $\Delta^{442–477}$::SG (**B**), *Is*PadC $\Delta^{514–516}$ (**F**), *Is*PadC $\Delta^{514–517}$ (**G**), and *Is*PadC $\Delta^{514–520}$ (**H**) obtained from the HPLC analysis of GTP conversion. Shown are the initial rates of product formation at different GTP concentrations. Product formation was quantified in triplicate for several reaction times and the standard deviation of individual points contributed to the error estimation of the linear fit that is used to calculate the initial rate of product formation. The standard error of the estimate from the linear regression is shown as error bar for each GTP concentration. The insets in all panels show a representative chromatogram of the HPLC analysis revealing the preferential formation of the linear pppGpG intermediate for *Is*PadC $\Delta^{514–516}$, while the other constructs show *Is*PadC-like c-di-GMP formation.

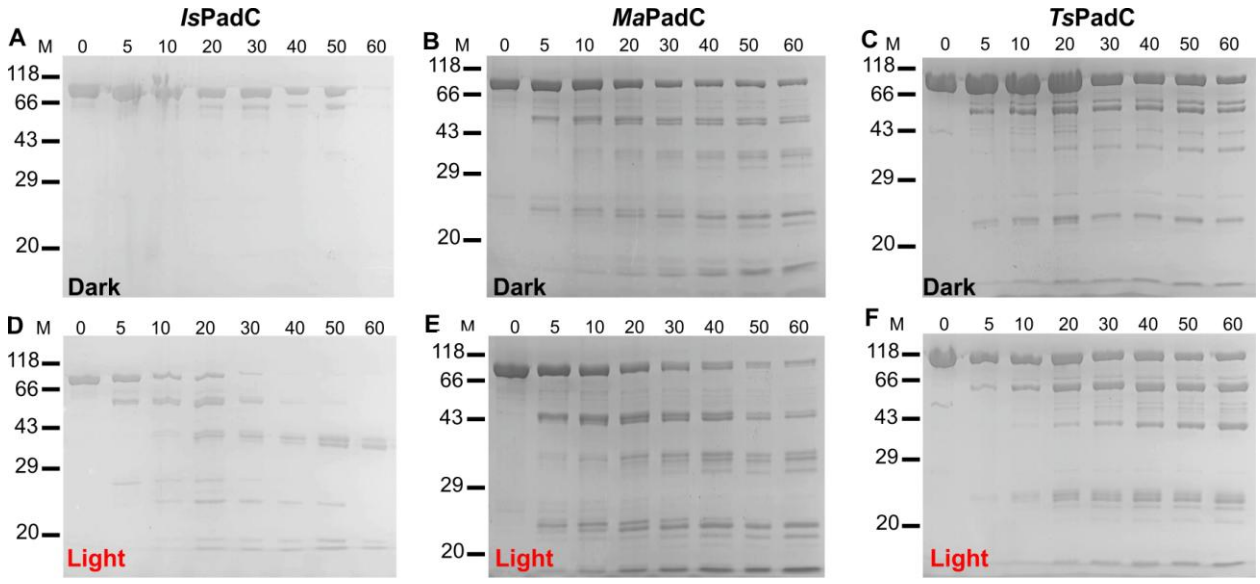

fig. S9. Time course of tryptic digests of *Is*PadC, *Ma*PadC, and *Ts*PadC under dark and light conditions. Panels (**A-C**) show Coomassie-blue stained 12% SDS-PAGE gels with 5µg of *Is*PadC, *Ma*PadC, and *Ts*PadC, respectively, loaded per lane after trypsin incubation in the dark over a total of 60 min. Panels (**D-F**) show the corresponding trypsin digestions with constant red light illumination over the same time frame. Ratios of trypsin to PadC differ for the various constructs and correspond to 1/100, 1/750 and 1/1000 for *Is*PadC, *Ma*PadC and *Ts*PadC, respectively.

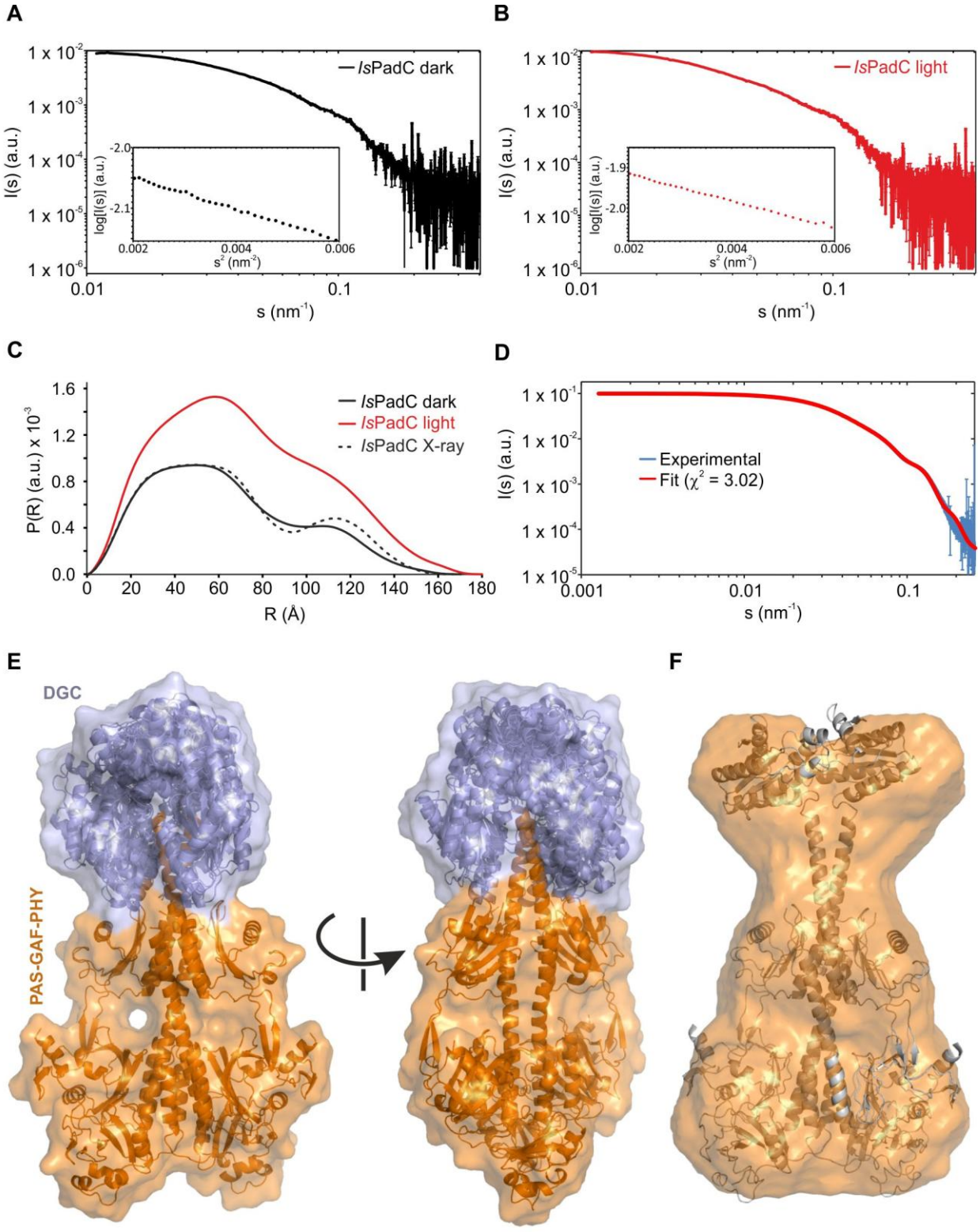

fig. S10. Details of SAXS measurements. (**A** and **B**) Raw SAXS data of dark and light-adapted *Is*PadC states, respectively. The insets show the corresponding Guinier plots, which demonstrate the absence of protein aggregation. Both, the s, and I(s) axes are shown in a logarithmic

representation. (**C**) SAXS data showing a comparison of the experimental radial density distributions of *Is*PadC in the dark- and light-state with a back-calculated radial density distribution from the crystal structure. SAXS-derived radius of gyration (R_g), maximal dimension (D_{max}), and molecular mass are 48.9 Å/160 Å /138 kDa for the dark and 55.9 Å/ 170 Å/237 kDa for the light-state, respectively. Transient oligomerization is frequently observed for phytochrome modules *(65)* and not directly linked to the DGC activation mechanism. For comparison SAXS data was back-calculated from the dark-state crystal structure using the program CRYSOL *(66)*. (**D**) Comparison of experimental *Is*PadC dark-state SAXS data with SAXS data back-calculated from the CORAL model. Both, the s, and I(s) axes are shown in a logarithmic representation. The angular ranges from 0.0012–0.3 nm^{-1} are compared. (**E**) Cartoon and surface representation of the bundle of 7 lowest energy structures from the SAXS-based rigid body modeling calculations of *Is*PadC in the dark-state. PAS-GAF-PHY and DGC domains are shown in orange and blue respectively. (**F**) SAXS-based *ab initio* low-resolution model of *Is*PadC superimposed with the crystal structure determined here.

table S1. Data collection, phasing, and refinement statistics.

	*Is*PadC Se-Met (PDB code: 5LLW)	*Is*PadC GTP soaked native (PDB code: 5LLX)	*Is*PadC PSMcc native (PDB code: 5LLY)
Data collection			
Space group	P 2_1 2_1 2_1	P 2_1 2_1 2_1	P 1 2_1 1
Cell dimensions			
a, *b*, *c* (Å)	50.87, 77.80, 439.98	50.73, 78.64, 452.04	83.70, 129.30, 122.28
α, β, γ (°)	90.0, 90.0, 90.0	90.0, 90.0, 90.0	90.0, 96.43, 90.0
Wavelength	0.979168	0.966	0.966
Resolution (Å)[a]	68.7 – 3.0 (3.1 – 3.0)	48.0 – 2.8 (2.9 – 2.8)	48.1 – 2.4 (2.5 – 2.4)
$R_{merge\ (\%)}$	13.2 (162.4)	18.4 (261.3)	7.1 (65)
$I/\sigma(I)$	15.85 (0.83)	7.81 (0.61)	10.31 (1.47)
$CC_{1/2}$	99.8 (29.6)	99.4 (14.2)	99.7 (62.7)
Completeness (%)	99.2 (99.7)	97.5 (99.3)	93.0 (94.1)
Redundancy	14.94 (3.93)	4.37 (4.55)	2.85 (2.80)
Refinement			
Resolution (Å)	68.7 – 3.0	48.0 – 2.8	48.1 – 2.4
No. reflections	67,329[b]	44,894	93,313
R_{work} / R_{free}	0.205 / 0.259	0.223 / 0.270	0.177 / 0.230
No. atoms			
Protein	10,850	10,647	16,287
Ligand/ion	86 / 2	150 / 4	184 / 8
Water	0	4	354
B factors			
Protein	98.0	92.7	59.0
Ligand/ion	73.9	80.2	48.0
Water	-	56.0	48.6
r.m.s deviations			
Bond lengths (Å)	0.010	0.009	0.008
Bond angles (°)	1.121	0.797	0.891

[a]Values in parentheses are for highest-resolution shell.

[b]Anomalous dataset: Friedel pairs are considered as different reflections.

table S2. Overview of oligonucleotides and buffers. (**A**) Oligonucleotides used in this study. (B) buffers used for purification and storage of the different PadC homologs.

Panel **A** - oligonucleotides

Desired construct	**Oligonucleotide (5′-3′)**
*Is*PadC $\Delta^{514–516}$	fw: gcagctgaatctgctgaatgatgatgcaaatgaaaatctggaaaaactggccag rv: atcattcagcagattcagctgcatgctatctgccacaatcagcagatcac
*Is*PadC $\Delta^{514–517}$	fw: gcagctgaatctgctgaatgatgcaaatgaaaatctggaaaaactggccagc rv: atcattcagcagattcagctgcatgctatctgccacaatcagcagatcac
*Is*PadC $\Delta^{514–520}$	fw: gcagctgaatctgctgaatgataatctggaaaaactggccagctttgatgatc rv: atcattcagcagattcagctgcatgctatctgccacaatcagcagatcac
*Is*PadC PSMcc	fw: ctggaaaaactggccagctaagcggccgcactcgagc rv: gctggccagtttttccagattttcatttgcatctgccagctgatc
*Is*PadC ccDGC	fw: cagctgaatctgctgaatgatcagctggcagatgcaaatgaaaatctg rv: gatcattcagcagattcagctgggcgccctgaaaataaagattctcag
*Is*PadC $\Delta^{442-477}$::SG	fw: acagagcggcagcggtaaaagccagccgtggcgtac rv: cgctgccgctctgtgcaacacgaaacagcagcagatagc
*Is*PadC register 1	fw: ctgaatctgctgaatgatcagctggcagatctaaatgaaaatctggaaaaactgg rv: ctgatcattcagcagattcagctgcatgctaagtgccacaatcagc
*Is*PadC register 2	fw: aatgatcagctggcagatgcaaatgaaaatctggaaaaactggtcagctttgatgatctg rv: catctgccagctgatcattcagcagattcagctgcatgacatctgccacaatc

Panel **B** – buffer systems

Use	**Homolog**	**Buffer composition**
Storage buffer	*Is*PadC	10 mM HEPES pH 7, 0.5 M NaCl, 2 mM $MgCl_2$
	*Ma*PadC	10 mM Tris/Cl pH 8, 0.5 M NaCl, 2 mM $MgCl_2$
	*Ts*PadC	10 mM Tris/Cl pH 8, 0.5 M NaCl, 2 mM $MgCl_2$
Lysis buffer	*Is*PadC	50 mM HEPES pH 7, 0.5 M NaCl, 2 mM $MgCl_2$, 10 mM imidazole, 1 mM EDTA
	*Ma*PadC	50 mM Tris/Cl pH 8, 0.5 M NaCl, 2 mM $MgCl_2$, 10 mM imidazole, 1 mM EDTA
	*Ts*PadC	50 mM Tris/Cl pH 8, 0.5 M NaCl, 2 mM $MgCl_2$, 10 mM imidazole, 1 mM EDTA
Dialysis buffer	*IsPadC*	50 mM HEPES pH 7, 0.5 M NaCl, 2 mM $MgCl_2$, 1 mM EDTA, 1 mM DTE
	MaPadC	50 mM Tris/Cl pH 8, 0.5 M NaCl, 2 mM $MgCl_2$, 1 mM EDTA, 1 mM DTE
	TsPadC	50 mM Tris/Cl pH 8, 0.5 M NaCl, 2 mM $MgCl_2$, 1 mM EDTA, 1 mM DTE

movie S1. Changes in conformational dynamics upon red light illumination of *Is*PadC. Animation of differential plots showing evaluated peptides from two HDX experiments (*Is*PadC$_{light}$ – *Is*PadC$_{dark}$) plotted onto the structure of *Is*PadC. Colors correspond to the bar legend in the animation with red indicating increased deuterium uptake in the light-state measurement of *Is*PadC. The time course represents the deuterium labeling times of 10, 45, 180, 900 and 3,600 seconds. See fig. S6**A** for details of peptides used in this animation and additional overlapping peptides.

movie S2. Changes in conformational dynamics upon red light illumination of the *Is*PadC PSMcc variant. Animation of differential plots showing evaluated peptides from two HDX experiments (*Is*PadC PSMcc$_{light}$ – *Is*PadC PSMcc$_{dark}$) plotted onto the part of the *Is*PadC structure that corresponds to the cloned PSMcc construct. Colors correspond to the bar legend in the animation. The time course corresponds to the deuterium labeling times of 10, 45, 180, 900 and 3,600 seconds. See fig. S6**B** for details of peptides used in this animation and additional overlapping peptides.

movie S3. The influence of effector deletion on conformational dynamics of the dark-state *Is*PadC PSMcc assembly. Animation of differential plots showing evaluated peptides from two HDX experiments (*Is*PadC$_{dark}$ – *Is*PadC PSMcc$_{dark}$) plotted onto the part of the *Is*PadC structure that corresponds to the cloned PSMcc construct. Colors correspond to the bar legend in the animation with blue indicating reduced deuterium uptake in the full length protein. The time course corresponds to the deuterium labeling times of 10, 45, 180, 900 and 3,600 seconds. See fig. S6**C** for details of peptides used in this animation and additional overlapping peptides.

movie S4. The influence of effector deletion on conformational dynamics of the light-state *Is*PadC PSMcc assembly. Animation of differential plots showing evaluated peptides from two HDX experiments (*Is*PadC$_{light}$ – *Is*PadC PSMcc$_{light}$) plotted onto the part of the *Is*PadC structure that corresponds to the cloned PSMcc construct. Colors correspond to the bar legend in the animation. The time course corresponds to the deuterium labeling times of 10, 45, 180, 900 and 3,600 seconds. See fig. S6**D** for details of peptides used in this animation and additional overlapping peptides.